High-pressure phase transitions of nitinol NiTi to a semiconductor with an unusual topological structure

Guangtao Liu, Hanyu Liu, Xiaolei Feng, and Simon A. T. Redfern

Phys. Rev. B **97**, 140104 — Published 26 April 2018

DOI: 10.1103/PhysRevB.97.140104

High-Pressure Phase Transitions of Nitinol, NiTi, to a Semiconductor with Unusual Topological Structure

Guangtao Liu[1], Hanyu Liu[2] , Xiaolei Feng[3] and Simon A. T. Redfern[3,4 *]

[1] *National Key Laboratory of Shock Wave and Detonation Physics, Institute of Fluid Physics, China Academy of Engineering Physics, Mianyang 621900, China*

[2] *Geophysical Laboratory, Carnegie Institution of Washington, Washington, DC 20015, USA*

[3] *Department of Earth Sciences, University of Cambridge, Downing Street, Cambridge, CB2 3EQ, UK*

[4] *Center for High Pressure Science and Technology Advanced Research, Shanghai 201203, China*

Abstract

Systematic *ab*-initio structure simulations have been used to explore the high-pressure behavior of nitinol (NiTi) at zero temperature. Our crystal structure prediction and first principles calculations reveal that the known B19 phase is dynamically unstable, an orthorhombic structure (*Pbcm*) and a face centered cubic B32 structure (*Fd*-3*m*) become stable above ~4 and 29 GPa, respectively. The newly-predicted, highest-pressure, B32 phase is composed of two interpenetrating diamond structures, with structural topology that is quite distinct from that of the other phases of NiTi. Interestingly, the B32 phase shows unusual semiconducting characteristic as a result of its unique band structure and the nature of 3*d* orbitals localization, whose expected synthesis pressure is accessible to current experimental techniques.

Key words: Nitinol, High Pressure, First Principles, Phase transition and Semiconductor.

Corresponding author: satr@cam.ac.uk (Simon A. T. Redfern)

I. Introduction

Nickel titanium (NiTi), termed nitinol, is widely used in automotive, aerospace, electronics and mechanical engineering as well as in medical devices. It is well-known for its shape memory and superelastic properties. Its shape memory behavior is driven by a reversible martensitic phase transition from a high-temperature austenitic B2 (*Pm*-3*m*) phase into a low-temperature martensitic phase[1,2] at around 273 K. Experimentally, single crystal x-ray diffraction[3,4] and powder neutron diffraction measurements[5] have determined the low-temperature phase as B19' ($P2_1/m$) with $\gamma \sim 97.8°$. Several experimental investigations have, however, reported the existence of multiple coexisting phases.[6–8] A large number of computational studies have been performed to uncover the underlying mechanism of phase transitions in NiTi.[9–16] *Ab* initio calculations revealed an additional orthorhombic B19 (*Pmma*) phase as well as an 'R-phase' (*P*3), which are both low-symmetry distortions of the high-symmetry B2 structure.[17] Density functional theory (DFT) calculations, in particular, have illuminated and explained the controversies about the energy surface and properties of NiTi, and have suggested results which are not always in agreement with the experimental observations. For example, the phonon frequencies of the experimentally-observed ambient B2 phase were calculated to be imaginary in conventional *ab*-initial calculation, indicating that this structure is dynamically unstable.[18] Moreover, the experimentally-observed low-temperature B19' structure was predicted to be unstable with respect to a higher-symmetry base-centered orthorhombic (BCO) B33 (*Cmcm*) structure at zero temperature[17], this B33 structure has not yet been confirmed in any experimental study, furthermore this space group precludes this phase from being a shape memory martensite alloy derived from the cubic structure. Many of these differences can be resolved if temperature-dependent entropic effects are taken into account in the calculations. For example, a recent theoretical study has showed that B2 and B19' structures are indeed stabilized, whereas the B33 structure is destabilized at finite temperature.[19]

Obviously, temperature factor plays a significant role in the martensitic structural phase transition of NiTi, leading to its shape memory effect, as underlined in both experimental and theoretical studies. But in addition to temperature, pressure also plays a controlling role in inducing such transitions by altering the crystal and/or electronic structures and generally pressure is well-recognized for creating novel structures and properties in materials, including metals and alloys. For example, a pressure-induced metal-semiconductor transition in lithium has been observed by direct electrical resistance measurements.[20] Transparent sodium was predicted by computational work, and then experimentally observed at high pressure, associated with pressure-induced *p*-*d* hybridization of valence electrons and their repulsion by core electrons into interstitial sites in the structure.[21] Further examples of pressure-induced structural transitions include that from disordered structure to a long-range face centered cubic (fcc) topological ordered structure in $Ce_{75}Al_{25}$, which was observed at 25 GPa[22]. The

ground-state phase of the prototype CoCrFeMnNi high-entropy alloy was retained during a high-pressure irreversible phase transition under compression.[23] Nowadays, pressure has been recognized and deployed as a very powerful and useful technique in the design, exploration and synthesis of novel functional materials. Following this path, the high-pressure properties and phase diagram of NiTi has been investigated using self-consistent *ab* initio lattice dynamical calculations which suggested that the B19' and B19 structures are stable high-pressure phases.[24]

In this work, we employ crystal structure predictions and first principles total energy calculations based on DFT, to further explore the high-pressure behavior of NiTi at zero temperature. Here, we find that the known B19 phase is dynamically unstable and report that the ground-state B33 phase transforms into a *Pbcm* phase at ~4 GPa, and finally to a B32 (*Fd*-3*m*) phase at ~29 GPa. Actually, we find that the predicted *Pbcm* phase is a distorted structure derived from the dynamically unstable B19 phase. The newly-uncovered B32 phase has a diamond-like stacking sequence, whose topological crystal structure is completely different from any previously-reported structural configuration of NiTi. The more intriguing prediction that the high-pressure B32 phase is a semiconductor with a narrow direct bandgap of ~0.26 eV, is a consequence of the special band structure associated with its unusual structural topology, which appears to be characterized by more localized 3*d* orbitals. Our findings indicate that metallic NiTi alloy displays a rich family of abundant structural phase transitions and will transform into an interestingly semiconducting state at high pressure, appears to show a new class of physical and chemical mechanisms of transformation for a transition metal alloys.

II. Computational details

The crystal structures of NiTi were probed systematically using the Crystal structure AnaLYsis by Particle Swarm Optimization (CALYPSO) code[25,26], which is based on a search for the global minimum in the free energy surfaces computed by the DFT total energy calculations. This method has been applied successfully to a wide range of crystalline systems ranging from elemental solids to binary and ternary compounds.[27–30] The simulation cell comprised 1 to 8 formula units (2-16 atoms) of NiTi at 0, 10 and 40 GPa. The population size of each generation was 50. The best 20 structures from last generation and 30 new ones generated by CALPYSO algorithm composed the next generation. Generally, the search was terminated after the generation of 2000-2500 structures.

DFT calculations, including structural optimizations, enthalpies, electronic structures and phonons, were performed using the Vienna Ab initio Simulation Package (VASP)[31] code employing the Perdew-Burke-Ernzerhof[32] exchange-correlation functional. The $3d^8 4s^2$ and $3d^2 3s^2$ electrons were treated as

valence electrons for Ni and Ti, respectively. Usually, the parameters of the structure searching are a little coarser than those of normal optimizations and enthalpy calculations to save CPU time, where energy cutoff is 400 eV and Monkhorst-Pack grid is $2\pi\times0.05$ Å^{-1} in reciprocal space here. We selected a lot of candidates (20-50) with low energy, then re-optimized all of them more precisely. To ensure that all enthalpy calculations were well converged, to about 1 meV/atom, a Monkhorst-Pack grid was selected with sufficient density ($2\pi\times0.05$ Å^{-1}) in reciprocal space, as well as appropriate energy cutoff (450 eV).[33]

The phonon calculations and modulation of soft phonon mode were carried out using a finite displacement approach[34] through the PHONOPY code[35], which uses the Hellmann-Feynman forces calculated from the optimized supercells through VASP code. In our calculations of phonon spectra, we selected $2\pi\times0.04$ Å^{-1} and 700 eV as the parameters and extended the unit cells to be big enough supercells with volume larger than ~ 1000 Å^3. For the B19 structure, the supercell is 3×4×3, including 144 atoms; for the *Pbcm* structure, the supercell is 3×4×1, including 96 atoms; and for the B32 structure, the supercell is 2×2×2, including 128 atoms.

III. Results and discussion

To validate our computational prediction method and DFT calculations in the NiTi system, using the CALYPSO search, we successfully reproduced the known ambient B2 phase, low-temperature B19' phase and the ground-state (0 K) B33 phase at atmospheric pressure, as well as their energy ordering: H(B2) > H(B19') > H(B33), verifying the reliability of our methodology. Then a new orthorhombic *Pbcm* phase and another cubic B32 phase were found during structure searching at 10 and 40 GPa, respectively. The enthalpy of each phase as a function of pressure is indicated in Figure 1. We find that the enthalpy of B33 phase is just a little lower than that of the B19' phase, which is consistent with previous studies.[19] The B33 phase is stable up to ~4 GPa, then transforms to the B19 phase or the *Pbcm* phase. It can be seen that it is very difficult to distinguish them on the basis of their energy, because the energy difference between these two primitive orthorhombic structures is less than the convergence accuracy of the energy calculation. At higher pressure (29 GPa), the B32 phase becomes enthalpically favored.

In addition to the enthalpy calculations for these structures, we have also calculated their phonon dispersion curves. The dynamic stabilities of the B33 phase and B19' phase have been confirmed in theoretical study previously.[19] For the B19 phase, we found a soft phonon branch with negative frequencies running from the Γ-point (0, 0, 0) to the Z-point (0, 0, 0.5) to the T-point (-0.5, 0, 0.5) of the Brillouin Zone (BZ) indicating that this structure is dynamically unstable. (Figure 2a) We therefore modulated the structure by introducing atomic

displacements corresponding to the wavevector of the Z-point within a supercell of the B19 structure and we obtained a *Pbcm* structure, which is the same structure as obtained in our crystal structure predictions. Actually, the crystal structure of the predicted *Pbcm* phase is a distorted supercell of the known B19 phase. Over the entire BZ, we found no imaginary phonon frequencies for this *Pbcm* phase nor for the B32 phase, confirming the dynamic stability of each of these two structures. (Figure 2b and 2c) We also confirmed their mechanical stabilities by computing the elastic constants.[33] Therefore, by considering both thermal and dynamical stabilities, it appears safe to conclude that, at zero temperature, the *Pbcm* phase and the B32 phase are calculated to be stable above ~4 and ~29 GPa, respectively.

In order to understand better the nature of the phase transitions between the high-pressure polymorphs of NiTi, we consider the crystal structures and details of these phases, as shown in Figure 3 and Table I. Careful observation of these NiTi crystal structures reveals that all of them, except the B32 phase, share the same structural topology. They can all be derived from the highly symmetric simple cubic B2 structure. In these phases, each Ti atom is eight-fold coordinated by Ni atoms and then regular or irregular hexahedra form their crystal structures. Both the temperature-induced martensitic phase transition (B2 → B19') and our newly-discovered pressure-induced phase transition (B33 → *Pbcm*) can be seen in terms of the varying relative displacements of Ni and Ti atoms, derived from a (seriously) distorted B2 structure.

In contrast, the high-pressure B32 structure shows a completely different topological crystal structure, and can be viewed as two interpenetrating diamond structures separated by a vector of (0.5, 0.5, 0.5). Each Ti atom is tetrahedrally coordinated by four Ti atoms and by four Ni atoms at identical distances, thus forming a superstructure of the body centered cubic (bcc) lattice, which often occurs in certain intermetallic I-III compounds (LiAl, LiGa, NaTl) and I-IIB alloys (LiZn, LiCd).[36] Thus, it can be seen that the transformation to the B32 phase involves a significant topological rearrangement and is a reconstructive phase transition, in contrast with the others structural phase transitions in NiTi. Therefore, the energy barrier of reconstructive phase transition (*Pbcm* → B32) is expected to be significantly higher than that of the lower-pressure transition (B33 → *Pbcm*). Additionally, we have calculated the equation of states of all these NiTi structures.[33] We find that the B32 phase is significantly denser than the other phases due to the nature change from (distorted) bcc stacking to close-packed fcc one, further underlining the expectation that this phase becomes most stable at extreme pressure.

To further investigate the electronic properties of NiTi, the band structures and the density of states (DOS) of all phases were studied by first principles calculations. It is expected that the B2, B33, and *Pbcm* phases show metallic behavior, as in a typical alloy system, where the valence bands and conduction bands completely overlap

and the DOS at the Fermi level is very high.[33] However, our computational results indicate that the predicted B32 structure shows a bandgap. It is well known that DFT usually underestimates the bandgap of materials, and we thus employed the screened hybrid functional of Heyd, Scuseria, and Ernzerhof (HSE06)[37] to better determine the electronic properties of this structure. The modified band structure (Figure 4) clearly shows that the B32 phase shows semiconducting character with a direct bandgap of ~0.26 eV between the Γ and X points, which is consistent with its DOS. From the projected DOS, we find that most of the electronic states below the Fermi level are associated with Ni 3*d* electrons, but also partly by Ti 3*d* electrons and their *s*, *p* orbitals. In contrast, the conduction band is composed of mainly by Ti 3*d* electrons.

Here, the novel electronic properties of B32 phase may directly contribute to nature of it crystal structure, a Zintl phase. Usually, such structures are poor conductors or semiconductors. Normally, such phases are the products of a reaction between group I/II elements and any post-transition metal or metalloid. The classic Zintl phase, NaTl, displays complete electron transfer from the more electropositive Na to the more electronegative Tl, just as in genuine ionic salts such as NaCl.[38] It behaves likes a group IV element, and it forms a diamond network structure. Thus, the band structure and density of states have characteristics related to those of the tetrahedrally bonded IV-IV semiconductors. For example, a study of LiAl indicates that while the Li-Al bond is an ionically polarized covalent bond, the Al-Al bonds are metallic-like and the Li-Li interactions are essentially nonbonding. It was found that this system shows a semimetallic band structure.[39] Our Bader population analysis[40] reveals an electron transfer of ~0.88 *e* from Ti to Ni in the B32 phase. In this B32 phase Ti and Ni show, to first approximation, +1 and -1 valence states, respectively, akin to LiAl, and the B32 structure of NiTi shows an obvious bandgap.

IV. Conclusions

In summary, we performed systematically theoretical studies on the structural variability and associated physical properties of NiTi alloy at high pressures. Through structure prediction method and first principles calculations, at zero temperature, we identify that its ground-state B33 phase transforms into a predicted higher-pressure *Pbcm* phase, and then to a highly symmetric B32 phase under increased compression. Further DFT studies reveal that the newly-uncovered B32 phase of this NiTi alloy shows an interestingly semiconducting behavior, which is associated with its special topological phase transition and the characteristic of 3*d* electrons. The present study provides new insights into the exploration and design of distinctive alloy materials under extreme condition.

ACKNOWLEDGEMENT

The authors acknowledge funding supports from the National Natural Science Foundation of China under Grants No. 11604314. Work at Carnegie was supported by Energy Frontier Research in Extreme Environments Center (EFree), an Energy Frontier Research Center funded by the Department of Energy (DOE), Office of Science, Basic Energy Sciences under Award No. DE-SC-0001057. S.A.T.R. acknowledges the support of the UK Natural Environment Research Council under grant NE/P012167/1.

Figures and captions:

Table I. The calculated crystal structure information of NiTi at different pressures.

Space group	Pressure (GPa)	Lattice parameters (Å)	Atoms	*x*	*y*	*z*
Pm-3*m* (B2)	0	*a* = 3.003	Ti	0.5	0.5	0.5
			Ni	0	0	0
$P2_1/m$ (B19')	0	*a* = 4.687 *b* = 4.038 *c* = 2.930 *β* = 98.97°	Ti	0.2189	0.25	0.0127
			Ni	0.6746	0.25	0.0491
Cmcm (B33/BCO)	0	*a* = 2.888 *b* = 9.398 *c* = 4.042	Ti	0	0.1440	0.75
			Ni	0	0.5847	0.25
Pmma (B19)	20	*a* = 4.176 *b* = 2.578 *c* = 4.505	Ti	0.25	0	0.2923
			Ni	0.25	0.5	0.8172
Pbcm	20	*a* = 2.572 *b* = 9.029 *c* = 4.176	Ti	0.0528	0.3975	0.25
			Ni	0.5357	0.1598	0.25
Fd-3*m* (B32)	40	*a* =5.585	Ti	0.5	0.5	0
			Ni	0	0	0.5

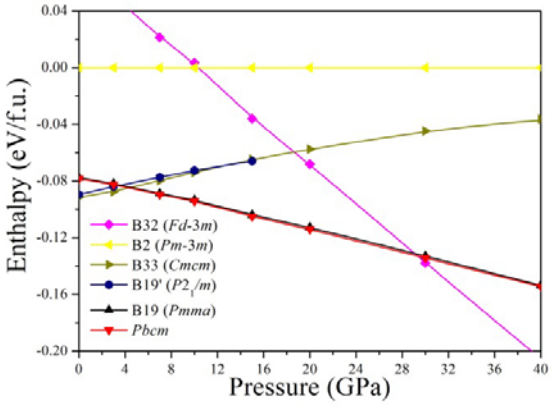

Figure 1: The calculated enthalpy as a function of pressure for each NiTi structure.

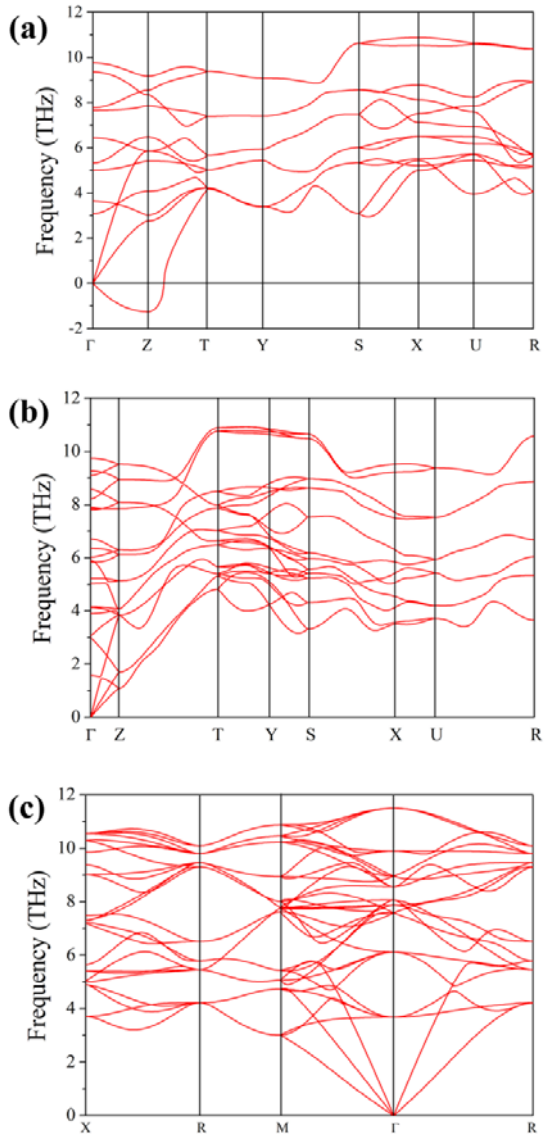

Figure 2: The phonon dispersions of NiTi in its (a) B19 structure at 20 GPa, (b) *Pbcm* structure at 20 GPa, (c) B32 structure at 40 GPa.

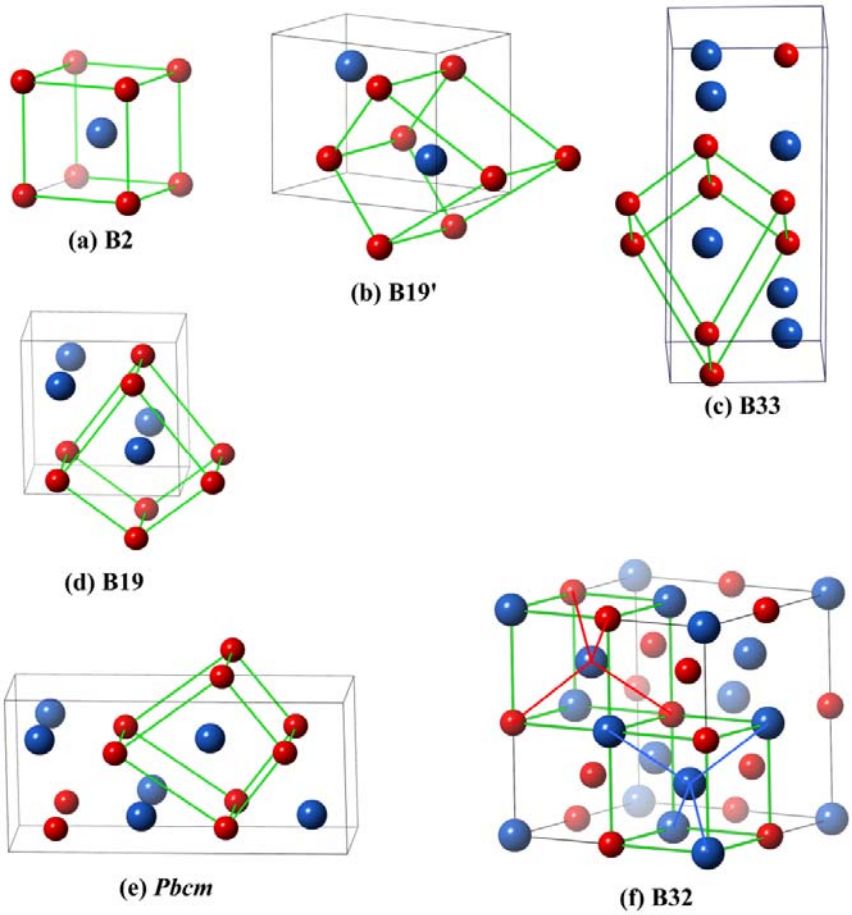

204

205 Figure 3: The schematic crystal structures of the NiTi phases (a) B2, (b) B19', (c) B33, (d) B19, (e) *Pbcm* and (f)

206 B32. Large blue and small red spheres represent Ni and Ti atoms, respectively.

207

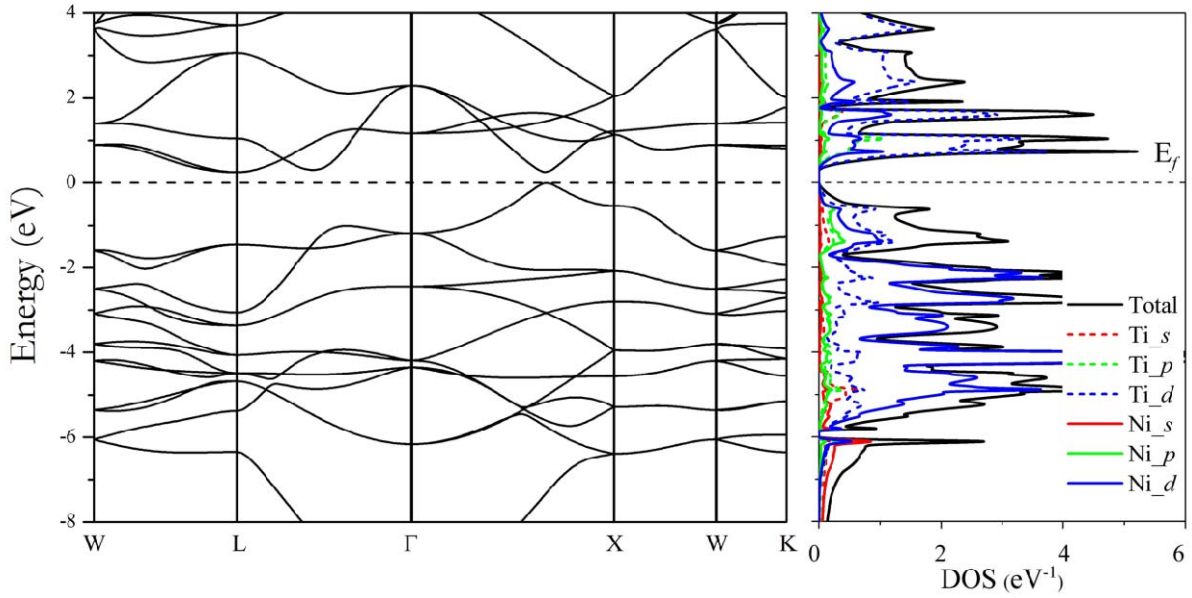

208

209 Figure 4: Band structure along high symmetry path and the projected DOS of the B32 structure at 40 GPa. The

210 Fermi level has been set to 0 eV.

211

References:

[1] Shaw John A and S. Kyriakides, J. Mech. Phys. Solids **43**, 1243 (1995).

[2] O. Benafan, S. A. P. II, R. D. Noebe, T. A. Sisneros, and R. Vaidyanathan, J. Appl. Phys. **112**, 93510 (2012).

[3] Y. Kudoh, M. Tokonami, and K. Otsuka, Acta Met. **33**, 2049 (1985).

[4] G. M. Michal and R. Sinclair, Acta Crystallogr. Sect. B Struct. Crystallogr. Cryst. Chem. **18**, 1803 (1981).

[5] H. Search, C. Journals, A. Contact, M. Iopscience, and I. P. Address, J. Phys. F Met. Phys. **13**, L77 (1983).

[6] P. Taylor, M. J. Marcinkowski, A. S. Sastri, and D. Koskimaki, Philos. Mag. **18**, 945 (1968).

[7] J. M. Carpenter, Acta Met. Mater **38**, 1291 (1990).

[8] F. E. Wang, S. J. Pickart, and H. A. Alperin, J. Appl. Phys **43**, 97 (1972).

[9] J. Wang and H. Sehitoglu, Appl. Phys. Lett. **101**, 81907 (2012).

[10] A. Pasturel, C. Colinet, D. N. Manh, A. T. Paxton, and M. van Schilfgaarde, Phys. Rev. B **52**, 15176 (1995).

[11] X. Huang, C. Bungaro, V. Godlevsky, and K. M. Rabe, Phys. Rev. B **65**, 14108 (2001).

[12] X. Wang, Phys. Rev. B **78**, 092103 (2008).

[13] N. Hatcher, O. Y. Kontsevoi, and A. J. Freeman, Phys. Rev. B **80**, 144203 (2009).

[14] N. Hatcher, O. Y. Kontsevoi, and A. J. Freeman, Phys. Rev. B **79**, 20202 (2009).

[15] D. Holec, M. Friak, A. Dlouhy, and J. Neugebauer, Phys. Rev. B **84**, 224119 (2011).

[16] K. G. Vishnu and A. Strachan, Phys. Rev. B **85**, 14114 (2012).

[17] Huang Xiangyang, G. J. Ackland, and K. M. Rabe, Nat. Mater. **2**, 307 (2003).

[18] K. Parlinski, Phys. Rev. B **66**, 64307 (2002).

[19] J. B. Haskins, A. E. Thompson, and J. W. Lawson, Phys. Rev. B **94**, 214110 (2016).

[20] T. Matsuoka and K. Shimizu, Nature **457**, 186 (2009).

[21] Y. Ma, M. Eremets, A. R. Oganov, Y. Xie, I. Trojan, S. Medvedev, A. O. Lyakhov, M. Valle, and V. Prakapenka, Nature **458**, 182 (2009).

[22] Q. S. Zeng, H. Sheng, Y. Ding, L. Wang, W. Yang, J.-Z. Jiang, W. L. Mao, and and H.-K. Mao, Science. **332**, 1404 (2012).

[23] F. Zhang, Y. Wu, H. Lou, Z. Zeng, V. B. Prakapenka, E. Greenberg, Y. Ren, J. Yan, J. S. Okasinski, X. Liu, Y. Liu, Q. Zeng, and Z. Lu, Nat. Commun. **8**, 1 (2017).

[24] C. Hu, Z. Zeng, Z. Niu, L. Cai, C. Kong, and Y. Cui, J. Alloys Compd. **608**, 258 (2014).

[25] Y. Wang, J. Lv, L. Zhu, and Y. Ma, Phys. Rev. B **82**, 94116 (2010).

[26] Y. Wang, J. Lv, L. Zhu, and Y. Ma, Comput. Phys. Commun. **183**, 2063 (2012).

[27] J. Lv, Y. Wang, L. Zhu, and Y. Ma, Phys. Rev. Lett. **106**, 15503 (2011).

[28] G. Liu, S. Besedin, A. Irodova, H. Liu, G. Gao, M. Eremets, X. Wang, and Y. Ma, Phys. Rev. B **95**, 104110 (2017).

[29] M. Zhang, H. Liu, Q. Li, B. Gao, Y. Wang, H. Li, C. Chen, and Y. Ma, Phys. Rev. Lett. **114**, 15502 (2015).

[30] Y. Li, J. Hao, H. Liu, S. Lu, and J. S. Tse, Phys. Rev. Lett. **115,** 105502 (2015).

[31] G. Kresse and J. Furthmüller, Phys. Rev. B **54**, 11169 (1996).

[32] E. M. PERDEW J, BURKE K, Phys. Rev. Lett. **77**, 3865 (1996).

[33] Supplementary Material

[34] K. Parlinski, Z. Q. Li, and Y. Kawazoe, Phys. Rev. Lett. **78,** 4063 (1997).

[35] A. Togo, F. Oba, and I. Tanaka, Phys. Rev. B **78,** 134106 (2008).

[36] M. Tadin, J. Schneider, H. Boysen, and F. Frey, Mater. Sci. Forum **79–82**, 635 (1991).

[37] J. Heyd, G. E. Scuseria, and M. Ernzerhof, J. Chem. Phys. **118**, 8207 (2003).

[38] S. C. Sevov, *Intermetallic Compounds – Principles and Practice – Volume 3: Progress* (2002).

[39] Z. Alex, Phys. Rev. B **17**, 2582 (1978).

[40] W. Tang, E. Sanville, and G. Henkelman, J. Phys. Condens. Matter **21**, 84204 (2009).